



UNIVERSITY OF LEEDS

This is a repository copy of *Global Uncertainty Propagation and Sensitivity Analysis in the CH₃OCH₂ + O₂ System: Combining Experiment and Theory To Constrain Key Rate Coefficients in DME Combustion*.

White Rose Research Online URL for this paper:
<https://eprints.whiterose.ac.uk/84293/>

Version: Accepted Version

Article:

Shannon, R, Tomlin, AS orcid.org/0000-0001-6621-9492, Robertson, S et al. (3 more authors) (2015) Global Uncertainty Propagation and Sensitivity Analysis in the CH₃OCH₂ + O₂ System: Combining Experiment and Theory To Constrain Key Rate Coefficients in DME Combustion. *The Journal of Physical Chemistry A*, 119 (28). pp. 7430-7438. ISSN 1089-5639

<https://doi.org/10.1021/acs.jpca.5b00620>

© 2015, American Chemical Society. This document is the Accepted Manuscript version of a Published Work that will appear in final form in *Journal of Physical Chemistry*, copyright © American Chemical Society after peer review and technical editing by the publisher. To access the final edited and published work see <http://dx.doi.org/10.1021/acs.jpca.5b00620>. Uploaded in accordance with the publisher's self-archiving policy.

Reuse

Items deposited in White Rose Research Online are protected by copyright, with all rights reserved unless indicated otherwise. They may be downloaded and/or printed for private study, or other acts as permitted by national copyright laws. The publisher or other rights holders may allow further reproduction and re-use of the full text version. This is indicated by the licence information on the White Rose Research Online record for the item.

Takedown

If you consider content in White Rose Research Online to be in breach of UK law, please notify us by emailing eprints@whiterose.ac.uk including the URL of the record and the reason for the withdrawal request.



eprints@whiterose.ac.uk
<https://eprints.whiterose.ac.uk/>

1
2
3 **Global Uncertainty Propagation and Sensitivity Analysis in the CH₃OCH₂ + O₂**
4
5
6 **System: Combining Experiment and Theory to Constrain Key Rate Coefficients**
7
8
9 **in DME Combustion**

10
11 R. J. Shannon^a, A. S. Tomlin^{*b}, S. H. Robertson^c, M. A. Blitz^a, M. J. Pilling^a, P. W. Seakins^a,

12
13 ^a School of Chemistry, University of Leeds, Leeds, LS2 9JT, UK

14
15 ^b Energy Research Institute, School of Chemical and Process Engineering, University of Leeds, Leeds,

16
17
18 LS2 9JT, UK

19
20 ^c Dassault Systèmes, BIOVA, Science Park, Cambridge, CB4 0WN, UK

21
22 * To whom correspondence should be addressed: A.S.Tomlin@leeds.ac.uk, tel: +44 113 3432500

Abstract

Statistical rate theory calculations, in particular formulations of the chemical master equation, are widely used in order to calculate rate coefficients of interest in combustion environments as a function of temperature and pressure. However despite the increasing accuracy of electronic structure calculations, small uncertainties in the input parameters for these master equation models can lead to relatively large uncertainties in the calculated rate coefficients. Master equation input parameters may be constrained further using experimental data and the relationship between experiment and theory warrants further investigation. In this work the $\text{CH}_3\text{OCH}_2 + \text{O}_2$ system, of relevance to the combustion of dimethyl ether (DME), is used as an example and the input parameters for master equation calculations on this system are refined through fitting to experimental data. Complementing these fitting calculations, global sensitivity analysis is used to explore which input parameters are constrained by which experimental conditions, and which parameters need to be further constrained in order to accurately predict key elementary rate coefficients. Finally, uncertainties in the calculated rate coefficients are obtained using both correlated and uncorrelated distributions of input parameters.

Key words: Master Equation; Sensitivity Analysis; Dimethyl Ether; Uncertainty Analysis; Correlation

Introduction

Theoretical calculations provide a useful way of estimating rate coefficients for systems over wide ranges of temperatures and pressures, some of which are inaccessible from experiments. However, several studies have recently demonstrated that errors, especially in calculated transition state energies, can lead to substantial uncertainties in predicted rate coefficients.^{1,2} These uncertainties have been suggested to be from a factor of two for simple abstraction reactions³, up to 5-10 for reactions in complex multi-well systems¹.

Experimental data can be used to substantially reduce the uncertainties in predicted rate coefficients by constraining the *ab initio* parameters^{4,5} and the exploitation of the complementary nature of experiment and theory warrants further exploration. In a recent publication⁶, extensive pulsed photolysis data for the $\text{CH}_3\text{OCH}_2 + \text{O}_2$ reaction were used to constrain the input parameters of a chemical master equation calculation using the implementation of the Levenberg-Marquardt algorithm for parameter optimisation within the open source MESMER code.⁷ This reaction system is a key step in the combustion of dimethyl ether (DME)⁸⁻¹³ and, with interest in the use of DME as a possible fuel¹⁴, the $\text{CH}_3\text{OCH}_2 + \text{O}_2$ reaction has attracted substantial attention.¹⁵⁻¹⁹ The experiments⁶ probed the reaction system by observation of OH, formed by dissociation of $\text{CH}_2\text{OCH}_2\text{OOH}$. Both the time dependence of OH formation and its yield were observed. Under the conditions of the experiment, the component of the OH growth associated with chemically activated product was closely related to the time dependence of the loss of CH_3OCH_2 by reaction with O_2 .

In this work, uncertainty propagation and global sensitivity analyses²⁰⁻²⁵ are reported for the $\text{CH}_3\text{OCH}_2 + \text{O}_2$ system, firstly in order to demonstrate how particular experiments can help to constrain the input parameters to the master equation, and secondly to explore the causes of remaining uncertainties following the fitting process. These sensitivity analyses were performed both for the conditions of existing experiments, and for conditions under which no experimental

1
2
3 data are available but which may be important from an applications perspective. This allows the
4
5 investigation of the relative importance of key parameters which control the uncertainty in rate
6
7 constant predictions under important combustion conditions, and hence how sensitivity analysis
8
9 could be used for the purposes of experimental design. In addition to the sensitivity analysis, we
10
11 assess the uncertainty in the elementary rate coefficients from the constrained master equation
12
13 calculations over conditions of relevance to practical devices, using both correlated and uncorrelated
14
15 input distributions.
16
17
18
19
20

21 **Methodology**

22 *Master equation (ME) calculations*

23
24
25 Figure 1 shows the stationary points on the potential energy surface for the $\text{CH}_3\text{OCH}_2 + \text{O}_2$ system.
26
27 Eskola et al. discussed these energies, obtained from a range of model chemistries, in a recent
28
29 publication.⁶ Although this previous publication found three transition states (TS) leading from
30
31 QOOH to $\text{OH} + 2\text{CH}_2\text{O}$, only the energy of the lowest of these transition states was varied in the
32
33 fitting calculations, and the energies of the other two TS were scaled such that the difference in
34
35 energies remained constant. This work utilises the same approach and the surface in Figure 1 is
36
37 simplified accordingly. Master equation calculations were performed using the open source
38
39 MESMER code^{7,26}, which has been discussed in a number of recent publications.^{13,27} Briefly, the
40
41 energies of the isomer adducts, RO_2 and QOOH, are divided into grains which are used as the basis of
42
43 the chemical master equation model. The form of the chemical master equation used is:
44
45
46
47

$$48 \quad \frac{d}{dt} \mathbf{p} = \mathbf{M} \mathbf{p} \quad (1)$$

49
50
51

52 where \mathbf{p} is a vector containing the populations, $p_i(E,t)$, of the energy grains and of the reactants,
53
54 where i refers to the i th isomer, and \mathbf{M} is the matrix that determines grain population evolution due
55
56 to collisional energy transfer within each isomer and reaction. Reactive processes, which include
57
58
59
60

1
2
3 isomerisation between RO₂ and QOOH, and dissociation from QOOH, are described by Rice
4
5 Ramsperger Kassel and Marcus (RRKM) theory, whilst collisional energy transfer is modelled using an
6
7 exponential down model parameterised by a temperature dependent $\langle \Delta E \rangle_{\text{down}}$, the average
8
9 amount of energy transferred in a downward direction upon collision with the bath gas. The
10
11 temperature dependence is described by the following expression:

$$\langle \Delta E \rangle_{\text{down}} = \langle \Delta E \rangle_{\text{down,ref}} \left(\frac{T}{T_{\text{ref}}} \right)^d \quad (2)$$

12
13
14
15
16
17
18
19 where $T_{\text{ref}} = 298$ K. Molecular densities of states were calculated assuming rigid external rotors and
20
21 harmonic oscillators, except for those modes best described as internal rotations. Modes
22
23 corresponding to internal rotations or torsions were modelled as hindered rotations and these
24
25 modes were projected out of the Hessian matrix according to the method of Sharma et al.²⁸ The CBS-
26
27 QB3//MPW1K/aug-cc-pVTZ frequencies, rotational constants and MPW1K/6-31+G hindrance
28
29 potentials for internal rotations from Eskola et al.⁶ were used in the current study.
30
31
32

33 For the barrierless association of CH₃OCH₂ with O₂, microcanonical rate coefficients were
34
35 calculated using an inverse Laplace transform (ILT) method assuming canonical high pressure limiting
36
37 rate coefficients of the form:

$$k_a(T) = A \left(\frac{T}{T_0} \right)^n \exp(-E_a / (k_B T)) \quad (3)$$

38
39
40
41
42
43
44
45 where, in the current case, the reference temperature T_0 is set to 195 K (the lowest temperature at
46
47 which experiments were performed) and the activation energy is set to zero in agreement with *ab*
48
49 *initio* calculations^{6,29,30} which show the association to be barrierless. The sensitivity of the calculated
50
51 rate coefficients to the A and n parameters will be explored in the current work. There is only one
52
53 hydrogen transfer process in this system corresponding to the isomerisation between RO₂ and
54
55
56
57
58
59
60

1
2
3 QOOH. Tunnelling was treated for this process using an Eckart methodology parametrised using the
4
5 imaginary frequency of the transition state TS1.³¹
6
7

8 It is important to distinguish between the energy dependent rate coefficients used in the
9
10 master equation and the pressure and temperature dependent rate coefficients derived from the
11
12 ME analysis. The former involve passage over a single transition state and are used in microcanonical
13
14 form. The latter are incorporated in the coupled sets of elementary reactions used in combustion
15
16 models. They are determined in the MESMER analysis using a method based on an approach
17
18 developed by Bartis and Widom.^{7,32} The resulting elementary reactions are shown in Figure 1. They
19
20 connect all species, and include so-called well-skipping reactions (e.g. R2, R3, R6) in which the
21
22 reaction system passes over more than one transition state and avoids stabilisation in an
23
24 intermediate well. These reactions and their associated rate coefficients emerge naturally from the
25
26 Bartis-Widom analysis; they are most important at lower pressures.
27
28
29
30
31

32 *Uncertainty propagation and global sensitivity analysis*

33
34 The uncertainties in the system parameters used in the master equation analysis were assessed in
35
36 two ways and global uncertainties within the inputs to the master equation model were propagated
37
38 using a sampling approach based on a quasi-random set of input samples.³³ For the initial, theory-
39
40 constrained approach, uncertainty ranges for the input parameters were based on theory
41
42 calculations alone, and typical of the type of analysis that might be performed in order to assist the
43
44 planning of experiments (see below). A Sobol low discrepancy sequence³³ was chosen for the
45
46 sampling, since it displays better convergence properties with respect to output statistics than more
47
48 traditional Monte Carlo pseudo random sequences. The inputs for each run were sampled from
49
50 uniform distributions that vary between the upper and lower limits discussed below and given in
51
52 Table 1. 2048 sample points were sufficient to derive accurate output distributions from the model.
53
54 The input-output relationships from these samples were subsequently used to perform a global
55
56 sensitivity analysis using the random sampling high dimensional model representation (RS-HDMR)
57
58
59
60

1
2
3 method.³⁴ The analysis was performed both for conditions of the proposed experiments and also for
4
5 conditions more typical of those found in combustion devices. In this way it is possible to explore
6
7 how the key parameters that determine the predictive uncertainty of rate constants calculated for
8
9 combustion conditions, can be constrained by the proposed experiments.
10

11
12 The first step of the theory-constrained analysis is to assign uncertainty ranges for the
13
14 parameters used in the master equation modelling as listed in Table 1. Experience from previous
15
16 systems can be used to estimate these theory-constrained uncertainties but realistically some expert
17
18 judgement has to be applied. For this work, we have made some use of the results of experimental
19
20 work to set the parameter ranges. Strictly speaking this is therefore not a truly a theory-constrained
21
22 calculation of sensitivity, but in planning experiments, one will generally have some limits on the
23
24 parameters from either previous studies on the same system, or studies of related systems.
25
26

27
28 The *ab initio* energies at the CBS-QB3 level of theory would usually be expected to exhibit
29
30 an uncertainty of $\sim 1 \text{ kcal mol}^{-1}$ (4.18 kJ mol^{-1})³ for stable species and this uncertainty was used for
31
32 the energies of RO_2 and QOOH . Transition states can be more problematic, and when discussing the
33
34 *ab initio* calculations in the work of Eskola et al.⁶ the authors pointed out that the transition state
35
36 TS2 in particular exhibited a large T1 diagnostic of 0.036 which is indicative of multireference effects.
37
38 The presence of such multi-reference effects is supported by the fact that a number of high level
39
40 model chemistries (G4, CBS-Q, CCSD(T)-f12) used in the calculations of Eskola et al.⁶ give very
41
42 different energies for the same species, varying by up to 40 kJ mol^{-1} in the case of TS2. Given the
43
44 complicated electronic structure in this region of the potential energy surface it is also possible that
45
46 other channels exist which were not discovered in the calculations performed by Eskola et al.⁶ In
47
48 view of these observations, larger uncertainty ranges were assigned to the transition state energies.
49
50

51
52
53 Since $\langle \Delta E \rangle_{\text{down}}$ is usually used as an empirical parameter, its uncertainty is estimated from
54
55 the typical range of $\langle \Delta E \rangle_{\text{down}}$ values with a helium bath gas³⁵. Helium is used as the bath gas,
56
57
58
59
60

1
2
3 because of the availability of more experimental data for this reaction system. Finally, uncertainty
4
5 ranges for the ILT parameters were assigned based upon intuition and upon high pressure limiting
6
7 association rate coefficients for other R + O₂ systems²⁷ whilst taking into account existing estimations
8
9 of the rate coefficient for CH₃OCH₂ + O₂^{9,11,18}.

10
11
12 The fitting of parameters to the experimental data of Eskola et al.⁶ was subsequently carried
13
14 out using the Levenberg-Marquardt non-linear least squares fitting routine within MESMER. In the
15
16 current work, the fits were carried out using the same experimental data as in the work by Eskola et
17
18 al.⁶, but the additional parameters, E(RO₂), E(QOOH) and ILT A were also allowed to vary. In the work
19
20 of Eskola et al.⁶ a detailed comparison was made of both a hindered rotor model and harmonic
21
22 oscillator only model for the system. Of the two models, the hindered one is the more physically
23
24 realistic and the differences such a model makes to the fitted parameters has already been discussed
25
26 in detail. For these reasons only the hindered model is considered in the current work.
27
28

29
30 The fitting procedure provides experimentally-constrained parameter ranges that are
31
32 independent of the theory-constrained ones and are based on the constraints imposed by the
33
34 experimental data alone. An ideal situation would be to carry out a third set of calculations
35
36 incorporating both experimental and theoretical constraints. However for the current work the aim
37
38 is to explore the differences between these two different approaches to sensitivity analysis and the
39
40 different kinds of information which can be obtained. Additionally, for this system, the prevalent
41
42 multi-reference effects make it particularly difficult to quantify the theory constrained uncertainty
43
44 ranges and in this case, given the extensive experimental dataset available, we would emphasise the
45
46 primacy of the experimental constraints.
47
48

49
50 Table 1 gives the upper and lower limits on each parameter from a joint probability
51
52 distribution created using the covariance matrix from the Levenberg-Marquardt fitting. The
53
54 covariance matrix is provided in the supplementary information and the related correlation matrix is
55
56 given in Table 2. The off-diagonal elements of the correlation matrix R_{ij} are given by:
57
58
59
60

$$R_{ij} = \frac{K_{ij}}{\sigma_i \sigma_j}$$

where K_{ij} are the corresponding elements of the covariance matrix.

These uncertainty ranges are significantly smaller than the proposed theory-constrained uncertainty ranges, for all parameters other than the energy of $\text{CH}_3\text{OCH}_2\text{O}_2$ ($E(\text{RO}_2)$) and the energy of $\text{CH}_2\text{CH}_2\text{OOH}$ ($E(\text{QOOH})$). A second global uncertainty propagation and sensitivity analysis was then performed using these experimentally-constrained uncertainties in order to explore how the sensitivities change when the large input ranges of the theory-constrained analysis are altered by the experimental constraints.

The global sensitivity analyses presented in this work utilise an HDMR method,^{34,36} as described previously.¹ Briefly the HDMR method uses a hierarchical function expansion to map the relationship between the input parameters x_1, \dots, x_n and output variables $f(\mathbf{x}) = f(x_1, \dots, x_n)$ of a model as follows:

$$f(\mathbf{x}) = f_0 + \sum_{i=1}^n f_i(x_i) + \sum_{1 \leq i < j \leq n} f_{ij}(x_i, x_j) \quad (4)$$

Here, we applied random sampling HDMR (RS-HDMR), where the functions $f_i(x_i)$ and $f_{ij}(x_i, x_j)$ in (4) are approximated by orthonormal polynomials fitted using a quasi-random sample of full model runs:

$$f_i(x_i) \approx \sum_{r=1}^k \alpha_r^i \varphi_r(x_i) \quad (5)$$

$$f_{ij}(x_i, x_j) \approx \sum_{p=1}^l \sum_{q=1}^{l'} \beta_{pq}^{ij} \varphi_p(x_i) \varphi_q(x_j)$$

where k, l, l' represent the order of the polynomial expansion, α_r^i and β_{pq}^{ij} are constant coefficients, and $\varphi_r(x_i)$, $\varphi_p(x_i)$ and $\varphi_q(x_j)$ are the orthonormal basis functions. For given input parameter ranges, the sensitivity indices indicate the relative contribution of each parameter to the predicted output

variance and can be used to explore interactions between parameters. To compute the sensitivity indices, the partial variances D_i and D_{ij} are calculated from the expansion coefficients:

$$D_i = \sum_{r=1}^{k_i} (\alpha_r^i)^2$$

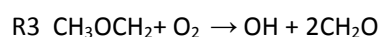
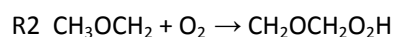
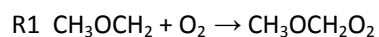
$$D_{ij} = \sum_{p=1}^{l_i} \sum_{q=1}^{l_j} (\beta_{pq}^{ij})^2$$
(6)

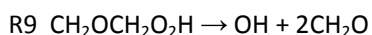
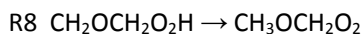
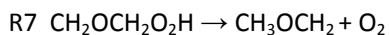
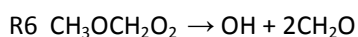
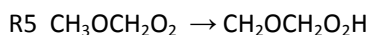
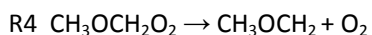
Finally, the sensitivity indices are calculated from $S_i = D_i/D$, $S_{ij} = D_{ij}/D$, where D is the total variance³⁷ given by:

$$D = \int_{K^n} f^2(x) dx - f_0^2$$
(7)

where $K^n = \{(x_1, \dots, x_n), i = 1, \dots, n\}$ represents an integral across the unit hypercube represented by the input Sobol sample. For the correlated experimentally-constrained sample, marginal indices are obtained as explained further in the results section.

The experimental data available for the $\text{CH}_3\text{OCH}_2 + \text{O}_2$ reaction consists of OH yields and rate coefficients for the overall loss of CH_3OCH_2 for temperatures between 195 K and 650 K and pressures from 5×10^2 Pa to 5×10^4 Pa. However key quantities of interest to the combustion community are rate coefficients for the elementary processes involved in the reaction. To reflect this, the sensitivity analyses have also been carried out using a number of the predicted elementary rate coefficients as outputs over a wider range of temperatures and pressures than covered by the experimental conditions. The purpose here is to establish how the errors in predicted rate coefficients from the constrained model, extrapolate to conditions of interest for modelling practical devices. The phenomenological reactions (R1 – R9) needed for a combustion model are shown in Figure 1 and are listed below.





18 *Generation of joint probability distribution*

19

20 The provision of confidence limits on the master equation observables for use by the modelling
21 community is particularly important for the elementary rate coefficients which have not been
22 directly validated by experiments. Confidence limits can be obtained by propagating errors
23 described by the input distributions with experimentally-constrained ranges from Table 1 and should
24 take into account correlations between parameters that result from the fitting. Joint probability
25 distributions, accounting for correlations, were obtained as described in Kucherenko et al.³⁸ A Sobol
26 sequence was first transformed into a standard normal vector $\tilde{\mathbf{x}}$ with zero mean and unit variance
27 using the inverse normal cumulative distribution function. A Cholesky decomposition of the
28 covariance matrix, Σ , from the Marquardt fitting was then calculated:
29
30
31
32

33
34
35
36
37
38
39
40
$$\Sigma = \mathbf{A}\mathbf{A}^T \quad (8)$$

41 and a joint probability distribution of the parameters \mathbf{x} was obtained from $\tilde{\mathbf{x}}$ as follows:

42
43
44
45
$$\mathbf{x} = \mathbf{A}\tilde{\mathbf{x}} + \boldsymbol{\mu} \quad (9)$$

46 Here $\boldsymbol{\mu}$ is a vector of the mean values for each parameter where each element μ_i is the mean value
47 for parameter i taken from the Marquardt fitting procedure. The full covariance matrix is available in
48 the supplementary information.
49
50
51
52

53 Using the joint probability distribution, uncertainty parameters, f , were obtained for R1-9 as
54 follows³⁹:
55
56
57
58
59
60

$$f = \log_{10} \left(\frac{k^{\mu} + 3\sigma}{k^{\mu}} \right) \quad (10)$$

where k^{μ} is the mean value of a given rate coefficient and σ is the standard deviation in the rate coefficient taken from the output distribution. The rate coefficient k can then be described as uncertain according to a multiplicative factor of 10^f .

Results

Theory-constrained Analysis

Using the theory-constrained ranges in conjunction with a Sobol sequence, distributions were obtained for the different rate coefficients and yields calculated using MESMER. Given the necessarily large ranges assigned it is not surprising that these distributions are wide, with f values up to 1.3 (i.e. uncertainties of up to a factor of 20). First- and second-order sensitivities for all eight parameters as listed in Table 1 were obtained using RS-HDMR. These are shown in the upper panel of Figure 2 for OH yields (Y) and CH₃OCH₂ loss rates (L) for a range of conditions. Mittal et al.¹¹ identified the elementary rate coefficients for R9 (QOOH decomposition to OH + 2CH₂O) and R5 (RO₂ → QOOH isomerization) to be particularly important in the low temperature combustion of DME, and Figure 2 also shows the sensitivities for these two elementary rate coefficients at 500, 700 and 900 K. In addition, the sensitivities for the elementary rate coefficients R6 (decomposition of RO₂ to OH + 2CH₂O) and R8 (isomerisation of QOOH back to RO₂) are also shown. Only the first-order and the major second-order indices are shown here and hence the total indices ($\sum S_i + \sum S_{i,j}$) may be less than unity in some cases.

Considering the yields, it was found that the two transition state energies E(TS1) (grey bars) and E(TS2) (orange bars) give the largest contributions to the predicted variance, through high first-order sensitivities and also via a large contribution from the second-order interaction term. As the pressure is decreased, the first-order sensitivity index for E(TS2) increases and that for E(TS1) decreases concomitantly. The large second-order sensitivity is likely due to the fact that the

1
2
3 uncertainty ranges for E(TS1) and E(TS2) are close to overlapping. These high sensitivities for E(TS1)
4 and E(TS2) suggest that experimental measurements of the yields would provide a high level of
5 constraint on these two parameters, and this is reflected to some extent in Table 1 that shows that
6 the post experimental uncertainty range for TS1 is significantly smaller than that for the other
7 energies.
8

9
10
11
12
13
14 Turning to the theory-constrained sensitivities of the CH₂OCH₃ loss rate, the ILT parameters
15 A (purple bars) and, to a lesser extent, *n* (green bars) dominate the sensitivities at lower
16 temperatures. At 650 K, the rate coefficients are more sensitive to E(TS1), E(TS2), and the energy
17 transfer parameters.
18
19
20

21
22 Given the large theory-constrained uncertainty ranges for E(TS1) and E(TS2), it is these
23 parameters which again dominate the sensitivities for the elementary rate coefficients, as shown in
24 the right hand panel in Figure 2. For the decomposition rate coefficients (R6 and R9) it is found that
25 E(TS2) is the dominant parameter since TS2 is the main bottleneck to product formation. Conversely
26 E(TS1) dominates the sensitivities for the two isomerisation steps R5 and R8. Since the transition
27 state energies dominate the uncertainty in both the OH yields and important rate constant
28 estimations, this suggests that measuring OH yields is critical to constraining the rate constants.
29 Further constraints on these transition states are also provided by measurements of CH₂OCH₃ loss
30 rates at higher temperatures. This sensitivity information therefore gives important information that
31 could be used in optimising experimental design.
32
33
34
35
36
37
38
39
40
41
42
43

44 In addition to yields and loss rates, experimental reciprocal time constants for OH formation
45 on a longer timescale are available from the work of Eskola et al.⁶ and these correspond to the
46 eigenvalue λ_1 from the master equation analysis in the 600 K to 650 K regime. These time constants
47 are associated with OH formation from the thermalised RO₂ species and from figure 2 it can be seen
48 that E(TS₂) dominates the sensitivities for these eigenvalues at both 650 and 600 K. This is
49 understandable since TS2 is the dominant bottleneck for this process. There is also some sensitivity
50
51
52
53
54
55
56
57
58
59
60

1
2
3 displayed to $E(\text{RO}_2)$ however this is less significant than in the $E(\text{TS}_2)$ case due to the much larger
4
5 uncertainty range on $E(\text{TS}_2)$.
6
7

8 9 *Experimentally-constrained Analysis*

10
11 The theory-constrained sensitivity analysis supports our previous work⁶ in demonstrating that,
12
13 despite the complications surrounding the *ab initio* calculation of the barrier heights, the energies of
14
15 the two transition states, TS_1 and TS_2 , can be well constrained by fitting master equations
16
17 calculations for $\text{CH}_3\text{OCH}_2 + \text{O}_2$ to the available experimental data. This is demonstrated by the
18
19 experimentally-constrained uncertainty ranges given in Table 1 for $E(\text{TS}_1)$ and $E(\text{TS}_2)$ which are
20
21 significantly narrower than the theory-constrained values. In the current work, all eight parameters
22
23 were defined through the Marquardt fitting procedure but we show that $E(\text{QOOH})$ is the least well
24
25 defined with an experimentally-constrained uncertainty range of 34 kJ mol^{-1} (Table 1).
26
27

28
29 A second set of sensitivity analyses was performed using the experimentally-constrained
30
31 uncertainty ranges in Table 1, allowing investigation of the causes of the remaining uncertainty in
32
33 the predictions from the master equation model. In the experimentally-constrained case, the
34
35 covariance matrix from the Marquardt calculations was used to create joint probability distributions
36
37 as described above. The marginal sensitivities for this correlated sample are shown in Figure 2 (lower
38
39 panel). These have again been calculated using RS-HDMR but in this case, because correlations are
40
41 present, the ordering of parameters within the transformations described in Eqs. (8) and (9) affects
42
43 the marginal sensitivities. Whilst this complicates the interpretation of the sensitivity indices
44
45 somewhat, ignoring correlations would lead to the decomposition of an artificially high output
46
47 variance and hence, whilst simpler to interpret, would give misleading results. For the interpretation
48
49 of marginal indices resulting from parameter correlations we follow the method of Mara and
50
51 Tarantola.⁴⁰ The sensitivity indices shown correspond to the full S_i for $E(\text{RO}_2)$ including its correlated
52
53 effects, the marginal S_i for $\langle \Delta E \rangle_{\text{down}}$ without its correlative contribution with $E(\text{RO}_2)$, the marginal
54
55
56
57
58
59
60

1
2
3 S_i for ILT A without its correlative contribution with $E(\text{RO}_2)$ and $\langle \Delta E \rangle_{\text{down}}$ and so on, following the
4
5 order given in Table 1. A full variance decomposition for correlated inputs providing all marginal
6
7 indices requires all permutations of the Cholesky decomposition to be used which is beyond the
8
9 scope of this paper. However, the marginal sensitivities for the ordering used here still provide
10
11 useful information which should be interpreted along with information from the covariance matrix.⁴⁰
12
13

14
15 Figure 2 shows that the energies of the two transition states no longer dominate the
16
17 sensitivities in the experimentally-constrained analysis. The yields now show large sensitivity indices
18
19 for $E(\text{RO}_2)$ (black bars) in particular, and also for $\langle \Delta E \rangle_{\text{down}}$ (red bars) with the marginal sensitivity
20
21 for $E(\text{TS1})$ now only becoming important at high temperatures and low pressures. The predicted loss
22
23 rates for CH_3OCH_2 are again dominated by ILT parameters at low temperatures but with the
24
25 temperature exponent, n , now the more important. $E(\text{TS1})$ has large sensitivity indices at higher
26
27 temperatures. It should be noted that $E(\text{RO}_2)$ and $E(\text{TS2})$ are strongly correlated as shown in Figure 3
28
29 and Table 2 and hence a strong sensitivity to $E(\text{RO}_2)$ also implies some sensitivity to $E(\text{TS2})$. The same
30
31 arguments can be applied to other input parameters which are highly correlated and the full
32
33 correlation matrix obtained from the covariance matrix (Table 2) indicated a high level of correlation
34
35 between the energies $E(\text{RO}_2)$, $E(\text{QOOH})$ (cyan bars) and $E(\text{TS2})$.
36
37

38
39 For the elementary rate coefficients $E(\text{RO}_2)$ is again the dominant parameter followed by
40
41 $\langle \Delta E \rangle_{\text{down}}$. These elementary rate coefficients are predominantly sensitive to the equilibrium
42
43 constant between RO_2 and QOOH . However when using the experimentally-constrained parameter
44
45 ranges and correlations for the current sample, it is $E(\text{RO}_2)$ which has the largest sensitivity index in
46
47 the majority of cases, although it is strongly correlated to $E(\text{QOOH})$. The elementary rate coefficient
48
49 for R9, the unimolecular decomposition of the QOOH to form $2\text{CH}_2\text{O} + \text{OH}$, exhibits the largest
50
51 marginal sensitivity indices for $E(\text{QOOH})$, and this is most constrained by the higher temperature
52
53 measurements of CH_3OCH_2 loss rates.
54
55
56
57
58
59
60

1
2
3 In the case of the eigenvalues λ_1 it is found that $E(\text{RO}_2)$ almost entirely dominates the
4 sensitivities. For these eigenvalues it is the energy gap between $E(\text{RO}_2)$ and $E(\text{TS2})$ which would be
5 expected to be the most important parameter and given that the post-experimental uncertainty
6 range for $E(\text{RO}_2)$ is larger than that for $E(\text{TS2})$, it is not surprising the $E(\text{RO}_2)$ displays the largest
7 sensitivity indices, however the extent to which this parameter dominates is exacerbated by the fact
8 that $E(\text{TS2})$ is strongly correlated to $E(\text{RO}_2)$ and thus, as noted above, the $E(\text{RO}_2)$ sensitivities could
9 also imply sensitivity to $E(\text{TS2})$.
10
11
12
13
14
15
16

17
18 From an experimental perspective, it is observables such as yields or total loss rates which
19 are the most amenable to measurement. However although they are not measured directly, it is the
20 elementary rate coefficients which are of most interest to the combustion modelling community.
21 Fitting input parameters to experiment is a vital tool in statistical rate theory allowing the predicted
22 elementary rate coefficients to be constrained by the available experimental quantities. In view of
23 this, sensitivity analysis for the data presented here for the experimentally determined variables
24 should be interpreted slightly differently to that for the elementary rate coefficients. The sensitivity
25 analysis data for the yields and total loss rate gives information regarding which experimental
26 conditions can be used to constrain which parameters, whereas the sensitivity data for the
27 elementary reactions demonstrate which parameters need to be further constrained in order to
28 reduce the uncertainty in these calculated values. The combination of the two sets of sensitivity data
29 provides vital insights into how experiments can be designed in order to best reduce uncertainties in
30 estimated rate constants under conditions of relevance to combustion simulations. The
31 experimental results of Eskola et al.⁶ constrain the key parameters $E(\text{RO}_2)$ and $E(\text{QOOH})$ relatively
32 poorly, because they are largely confined to low temperatures and relatively low pressures. The
33 present results show that more extensive experimental data at 500 K and above would constrain
34 these parameters further, and hence the rate coefficients for the key elementary reactions more
35 fully.
36
37
38
39
40
41
42
43
44
45
46
47
48
49
50
51
52
53
54
55
56
57
58
59
60

Uncertainty factors for elementary rate coefficients

Uncertainty parameters were obtained from both the correlated and uncorrelated experimentally-constrained distributions in order to estimate errors in the rate coefficients calculated using MESMER (Table 3). For the uncorrelated distributions all off diagonal terms in the covariance matrix were set to zero, purely for comparison purposes. The extent of the correlation between some parameters is shown in the joint probability distributions in Figures 3 and 4. These correspond to one pair of parameters which are highly correlated and one pair of parameters which are relatively independent with correlation matrix elements of 0.98 and -0.01 for $E(\text{RO}_2)$ and $E(\text{TS2})$ and for $E(\text{TS2})$ and $E(\text{TS1})$ respectively. These results highlight the importance of taking account of correlations between the fitted parameters in order not to overestimate the uncertainty factors. The analysis supports previous findings by Nagy and Turányi concerning the treatment of correlations in the uncertainty parameters for Arrhenius expressions.⁴¹⁻⁴³ The correlations will also affect the interpretation of the sensitivity information as highlighted above. A high total sensitivity to $E(\text{RO}_2)$ or $E(\text{TS2})$ will lead to a high sensitivity in the other because of their high correlation.

The uncertainties from the correlated sample in Table 3 show substantial reductions of up to a factor of 2 when compared to the corresponding ones from the uncorrelated sample. Under conditions typical of combustion applications (700, 900 K and 970, 1200 kPa), the uncertainty of the rate constant for the isomerisation reaction $\text{RO}_2 \rightarrow \text{QOOH}$ has an f factor of approximately 0.5 which implies uncertainties of around a factor of 3. The rate constant for $\text{QOOH} \rightarrow \text{OH} + 2\text{CH}_2\text{O}$ has a lower uncertainty which corresponds to around a factor of 2 for typical combustion conditions. Both of these reactions were highlighted as being extremely sensitive for low temperature predictions of DME combustion in both flow reactors and ignition studies by Tomlin et al.⁴⁴ Thus, providing better quantification of these rates is important for improving the robustness of low temperature combustion simulations of DME. Well skipping reactions develop naturally from the Bartis-Widom analysis of the master equation in the present study but have not been included in DME oxidation mechanisms to date. These reactions are fairly well constrained by the current study with

1
2
3 uncertainties of a factor of 2 or lower. The current study therefore provides useful data for the
4
5 improvement of DME oxidation mechanisms. The highest remaining uncertainties are for QOOH \rightarrow
6
7 RO₂, which directly affects the lifetime and concentration of QOOH and hence the rate of branching
8
9 in combustion systems, particularly at the lower temperatures. This may result from the poor
10
11 constraint of E(QOOH) by the current experiments.
12

13 14 15 16 **Conclusions**

- 17
18
19 1. We have demonstrated that the large amount of pulsed photolysis data available for the
20
21 CH₃OCH₂ + O₂ reaction can be used to constrain many of the key parameters used in master
22
23 equation modelling of the system. Sensitivity analysis using proposed theory-constrained
24
25 uncertainties supports our previous work in demonstrating how accurate experimental data
26
27 can constrain *ab initio* transition state energies in multiwell systems.
28
- 29
30 2. Repeating the sensitivity analyses with correlated samples from the Marquardt fitting to the
31
32 pulsed photolysis results highlights both which model parameters are constrained by which
33
34 experiments, and which parameters are important in the determination of key elementary
35
36 rate coefficients.
37
38
- 39
40 3. The low temperature experiments probing the time dependence of OH formation, and
41
42 hence the loss of CH₃OCH₂, were particularly successful in constraining the ILT parameters
43
44 for the initial reaction of CH₃OCH₂ with O₂. One important observation from both the theory-
45
46 and experimentally-constrained analyses is that in both cases the low temperature loss rates
47
48 are dominated by the ILT parameters. Quantities other than the loss rates display negligible
49
50 sensitivities to these parameters and this demonstrates how an ILT method can be
51
52 effectively parameterised by experimental measurements of loss rates even in cases where
53
54 the high pressure limit has not yet been achieved.
55
56
57
58
59
60

1
2
3 4. Referring to the theory constrained analyses, the sensitivity indices for the OH yield
4
5 experiments suggest that these data successfully constrain the energies of TS1 and TS2. The
6
7 reduced theory constrained uncertainty ranges for these parameters compared to E(QOOH)
8
9 and E(RO₂) support this observation. Through constraints on E(TS1) and E(TS2) these
10
11 experiments reduce uncertainties in predicted rate coefficients for the decomposition
12
13 reactions of QOOH and RO₂ to OH + 2CH₂O, particularly at higher temperatures.
14
15

16
17 5. Fits to the experimental data, were less successful in constraining energies for RO₂ and
18
19 QOOH although post experiment analyses show high sensitivity to E(RO₂). The energy of
20
21 QOOH, which is important in branching steps in low temperature combustion, is poorly
22
23 constrained by the experimental data available.
24
25

26
27 The key elementary rate coefficients, as shown in the right hand panels in Figure 2 appear
28
29 more sensitive to E(RO₂) than E(QOOH). However, there are strong correlations between
30
31 E(RO₂), E(TS2) and E(QOOH) (Table 2), which may imply strong joint sensitivities.
32

33
34 6. Given the importance of QOOH in low temperature combustion, the low marginal sensitivity
35
36 to E(QOOH) and E(TS2) shown in the post-experiment analysis demonstrates the need for a
37
38 wider range of experimental conditions. E(QOOH) is most sensitive to experiments at higher
39
40 temperatures, via the loss rates of CH₃OCH₂ in particular. However, through its correlation
41
42 with E(RO₂), as discussed above, this parameter is still likely to influence rate constant
43
44 predictions. By performing experiments across a range of temperatures and pressures, the
45
46 marginal effects of these two parameters could be further constrained since E(RO₂)
47
48 dominates for lower temperature OH yields and E(QOOH) for higher temperature CH₃OCH₂
49
50 loss rates. E(RO₂) is particularly sensitive to λ_1 and experiments over a range of
51
52 temperatures should provide improved constraints.
53
54
55
56
57
58
59
60

1
2
3 7. In addition to the sensitivity analysis, the work demonstrates the importance of accounting
4 for correlations between input parameters when estimating predictive errors, since
5 otherwise the uncertainties on theoretically predicted rate coefficients can be substantially
6 overestimated. The remaining uncertainties within the constrained master equation model
7 for two key elementary reaction rate coefficients were found to be between factors of 1.3
8 and 3.5 depending upon the conditions.
9
10
11
12
13
14
15
16
17
18
19

20 Acknowledgements

21
22 The authors would like to acknowledge the EPSRC (grant EP/J010871/1) for funding.
23
24

25 Supporting Information Available

26
27 A table detailing the covariance matrix from the Levenberg-Marquardt fitting is available in
28 supporting information. This information is available free of charge via the Internet at
29 <http://pubs.acs.org>
30
31
32
33
34
35

36 References

- 37
38
39 (1) Goldsmith, C. F.; Tomlin, A. S.; Klippenstein, S. J. Uncertainty Propagation in the
40 Derivation of Phenomenological Rate Coefficients from Theory: A Case Study of N-Propyl Radical
41 Oxidation. *Proc. Combust. Inst.* **2013**, *34*, 177-185.
42 (2) Klippenstein, S. J.; Harding, L. B.; Davis, M. J.; Tomlin, A. S.; Skodje, R. T. Uncertainty
43 Driven Theoretical Kinetics Studies for CH₃OH Ignition: HO₂+CH₃OH and O₂+CH₃OH. *Proc. Combust.*
44 *Inst.* **2011**, *33*, 351-357.
45 (3) Curtiss, L. A.; Redfern, P. C.; Raghavachari, K. Assessment of Gaussian-4 Theory for
46 Energy Barriers. *Chem. Phys. Lett.* **2010**, *499*, 168-172.
47 (4) Prager, J.; Najm, H. N.; Zador, J. Uncertainty Quantification in the *Ab Initio* Rate-
48 Coefficient Calculation for the CH₃CH(OH)CH₃ + OH → CH₃C(OH)CH₃ + H₂O Reaction. *Proc. Combust.*
49 *Inst.* **2013**, *34*, 583-590.
50 (5) Burke, M. P.; Klippenstein, S. J.; Harding, L. B. A Quantitative Explanation for the
51 Apparent Anomalous Temperature Dependence of OH + HO₂ = H₂O + O₂ through Multi-Scale
52 Modeling. *Proc. Combust. Inst.* **2013**, *34*, 547-555.
53 (6) Eskola, A. J.; Carr, S. A.; Shannon, R. J.; Wang, B.; Blitz, M. A.; Pilling, M. J.; Seakins, P.
54 W.; Robertson, S. H. Analysis of the Kinetics and Yields of OH Radical Production from the CH₃OCH₂ +
55 O₂ Reaction in the Temperature Range 195-650 K: An Experimental and Computational Study. *J. Phys.*
56 *Chem. A* **2014**, *118*, 6773-6788.
57
58
59
60

- (7) Glowacki, D. R.; Liang, C. H.; Morley, C.; Pilling, M. J.; Robertson, S. H. MESMER: An Open-Source Master Equation Solver for Multi-Energy Well Reactions. *J. Phys. Chem. A* **2012**, *116*, 9545-9560.
- (8) Zador, J.; Taatjes, C. A.; Fernandes, R. X. Kinetics of Elementary Reactions in Low-Temperature Autoignition Chemistry. *Progress in Energy and Combustion Science* **2011**, *37*, 371-421.
- (9) Curran, H. J.; Fischer, S. L.; Dryer, F. L. The Reaction Kinetics of Dimethyl Ether. II: Low-Temperature Oxidation in Flow Reactors. *Int. J. Chem. Kinet.* **2000**, *32*, 731-759.
- (10) Curran, H. J.; Pitz, W. J.; Westbrook, C. K.; Dagaut, P.; Boettner, J. C.; Cathonnet, M. A Wide Range Modeling Study of Dimethyl Ether Oxidation. *Int. J. Chem. Kinet.* **1998**, *30*, 229-241.
- (11) Mittal, G.; Chaos, M.; Sung, C. J.; Dryer, F. L. Dimethyl Ether Autoignition in a Rapid Compression Machine: Experiments and Chemical Kinetic Modeling. *Fuel Processing Technology* **2008**, *89*, 1244-1254.
- (12) Bansch, C.; Kiecherer, J.; Szori, M.; Olzmann, M. Reaction of Dimethyl Ether with Hydroxyl Radicals: Kinetic Isotope Effect and Prereactive Complex Formation. *J. Phys. Chem. A* **2013**, *117*, 8343-8351.
- (13) Carr, S. A.; Still, T. J.; Blitz, M. A.; Eskola, A. J.; Pilling, M. J.; Seakins, P. W.; Shannon, R. J.; Wang, B.; Robertson, S. H. Experimental and Theoretical Study of the Kinetics and Mechanism of the Reaction of OH Radicals with Dimethyl Ether. *J. Phys. Chem. A* **2013**, *117*, 11142-11154.
- (14) Ribeiro, N. M.; Pinto, A. C.; Quintella, C. M.; da Rocha, G. O.; Teixeira, L. S. G.; Guarieiro, L. L. N.; Rangel, M. D.; Veloso, M. C. C.; Rezende, M. J. C.; da Cruz, R. S. et al. The Role of Additives for Diesel and Diesel Blended (Ethanol or Biodiesel) Fuels: A Review. *Energy Fuels* **2007**, *21*, 2433-2445.
- (15) Maricq, M. M.; Sente, J. J.; Hybl, J. D. Kinetic Studies of the Oxidation of Dimethyl Ether and Its Chain Reaction with Cl₂. *J. Phys. Chem. A* **1997**, *101*, 5155-5167.
- (16) Rosado-Reyes, C. M.; Francisco, J. S.; Sente, J. J.; Maricq, M. M.; Ostergaard, L. F. Dimethyl Ether Oxidation at Elevated Temperatures (295-600 K). *J. Phys. Chem. A* **2005**, *109*, 10940-10953.
- (17) Eskola, A. J.; Carr, S. A.; Blitz, M. A.; Pilling, M. J.; Seakins, P. W. Kinetics and Yields of OH Radical from the CH₃OCH₂ + O₂ Reaction Using a New Photolytic Source. *Chem. Phys. Lett.* **2010**, *487*, 45-50.
- (18) Andersen, A.; Carter, E. A. First-Principles-Derived Kinetics of the Reactions Involved in Low-Temperature Dimethyl Ether Oxidation. *Mol. Phys.* **2008**, *106*, 367-396.
- (19) Yamada, T.; Bozzelli, J. W.; Lay, T. H. Comparisons of CBS-Q and G2 Calculations on Thermodynamic Properties, Transition States, and Kinetics of Dimethyl-Ether Plus O₂ Reaction System. *Int. J. Chem. Kinet.* **2000**, *32*, 435-452.
- (20) Skodje, R. T.; Tomlin, A. S.; Klippenstein, S. J.; Harding, L. B.; Davis, M. J. Theoretical Validation of Chemical Kinetic Mechanisms: Combustion of Methanol. *J. Phys. Chem. A* **2010**, *114*, 8286-8301.
- (21) Turanyi, T.; Zalotai, L.; Dobe, S.; Berces, T. Effect of the Uncertainty of Kinetic and Thermodynamic Data on Methane Flame Simulation Results. *Physical Chemistry Chemical Physics* **2002**, *4*, 2568-2578.
- (22) Zador, J.; Zsely, I. G.; Turanyi, T. Local and Global Uncertainty Analysis of Complex Chemical Kinetic Systems. *Reliability Engineering & System Safety* **2006**, *91*, 1232-1240.
- (23) Ziehn, T.; Hughes, K. J.; Griffiths, J. F.; Porter, R.; Tomlin, A. S. A Global Sensitivity Study of Cyclohexane Oxidation under Low Temperature Fuel-Rich Conditions Using HDMR Methods. *Combustion Theory and Modelling* **2009**, *13*, 589-605.
- (24) Ziehn, T.; Tomlin, A. S. A Global Sensitivity Study of Sulfur Chemistry in a Premixed Methane Flame Model Using HDMR. *Int. J. Chem. Kinet.* **2008**, *40*, 742-753.
- (25) Zsely, I. G.; Zador, J.; Turanyi, T. Uncertainty Analysis of NO Production During Methane Combustion. *Int. J. Chem. Kinet.* **2008**, *40*, 754-768.

- 1
2
3 (26) Bossmeyer, J.; Brauers, T.; Richter, C.; Rohrer, F.; Wegener, R.; Wahner, A.
4 Simulation Chamber Studies on the NO₃ Chemistry of Atmospheric Aldehydes. *Geophys. Res. Lett.*
5 **2006**, *33*, L18810.
- 6 (27) Carr, S. A.; Glowacki, D. R.; Liang, C. H.; Baeza-Romero, M. T.; Blitz, M. A.; Pilling, M.
7 J.; Seakins, P. W. Experimental and Modeling Studies of the Pressure and Temperature
8 Dependences of the Kinetics and the OH Yields in the Acetyl + O₂ Reaction. *J. Phys. Chem. A* **2011**,
9 *115*, 1069-1085.
- 10 (28) Sharma, S.; Raman, S.; Green, W. H. Intramolecular Hydrogen Migration in
11 Alkylperoxy and Hydroperoxyalkylperoxy Radicals: Accurate Treatment of Hindered Rotors. *J. Phys.*
12 *Chem. A* **2010**, *114*, 5689-5701.
- 13 (29) Andersen, A.; Carter, E. A. Hybrid Density Functional Theory Predictions of Low-
14 Temperature Dimethyl Ether Combustion Pathways. II. Chain-Branching Energetics and Possible Role
15 of the Criegee Intermediate. *J. Phys. Chem. A* **2003**, *107*, 9463-9478.
- 16 (30) Suzaki, K.; Takahisa, C.; Tsuchiya, K.; Koshi, M.; Tezaki, A. Formation Pathways of
17 HO₂ and OH Changing as a Function of Temperature in Photolytically Initiated Oxidation of Dimethyl
18 Ether. *Proc. Combust. Inst.* **2007**, *31*, 295-303.
- 19 (31) Miller, W. H. Tunneling Corrections to Unimolecular Rate Constants, with
20 Application to Formaldehyde. *J. Am. Chem. Soc.* **1979**, *101*, 6810-6814.
- 21 (32) Bartis, J. T.; Widom, B. Stochastic-Models of Interconversion of 3 or More Chemical
22 Species. *J. Chem. Phys.* **1974**, *60*, 3474-3482.
- 23 (33) Sobol, I. On the Distribution of Points in a Cube and the Approximation Evaluation
24 of Each Integrals. *Comp Math Math Phys* **1976**, *7*, 86-112.
- 25 (34) Ziehn, T.; Tomlin, A. S. Gui-HDMR - a Software Tool for Global Sensitivity Analysis of
26 Complex Models. *Environmental Modelling & Software* **2009**, *24*, 775-785.
- 27 (35) Holbrook, K. A.; Pilling, M. J.; Robertson, S. H.; Robinson, P. J. *Unimolecular*
28 *Reactions*, 2nd ed.; Wiley: Chichester ; New York, 1996.
- 29 (36) Rabitz, H.; Alis, O. F.; Shorter, J.; Shim, K. Efficient Input-Output Model
30 Representations. *Computer Physics Communications* **1999**, *117*, 11-20.
- 31 (37) Li, G. Y.; Wang, S. W.; Rabitz, H.; Wang, S. Y.; Jaffe, P. Global Uncertainty
32 Assessments by High Dimensional Model Representations (HDMR). *Chemical Engineering Science*
33 **2002**, *57*, 4445-4460.
- 34 (38) Kucherenko, S.; Tarantola, S.; Annoni, P. Estimation of Global Sensitivity Indices for
35 Models with Dependent Variables. *Computer Physics Communications* **2012**, *183*, 937-946.
- 36 (39) Nagy, T.; Turanyi, T. Reduction of Very Large Reaction Mechanisms Using Methods
37 Based on Simulation Error Minimization. *Combustion and Flame* **2009**, *156*, 417-428.
- 38 (40) Mara, T. A.; Tarantola, S. Variance-Based Sensitivity Indices for Models with
39 Dependent Inputs. *Reliability Engineering & System Safety* **2012**, *107*, 115-121.
- 40 (41) Nagy, T.; Turanyi, T. Uncertainty of Arrhenius Parameters. *Int. J. Chem. Kinet.* **2011**,
41 *43*, 359-378.
- 42 (42) Nagy, T.; Turanyi, T. Determination of the Uncertainty Domain of the Arrhenius
43 Parameters Needed for the Investigation of Combustion Kinetic Models. *Reliability Engineering &*
44 *System Safety* **2012**, *107*, 29-34.
- 45 (43) Turanyi, T.; Nagy, T.; Zsely, I. G.; Cserhati, M.; Varga, T.; Szabo, B. T.; Sedyo, I.; Kiss, P.
46 T.; Zemleni, A.; Curran, H. J. Determination of Rate Parameters Based on Both Direct and Indirect
47 Measurements. *Int. J. Chem. Kinet.* **2012**, *44*, 284-302.
- 48 (44) Tomlin, A. S.; Agbro, E.; Nevrlly, V.; Dlabka, J.; Vasinek, M. Evaluation of Combustion
49 Mechanisms Using Global Uncertainty and Sensitivity Analyses: A Case Study for Low-Temperature
50 Dimethyl Ether Oxidation. *Int. J. Chem. Kinet.* **2014**, *46*, 662-682.
- 51
52
53
54
55
56
57
58
59
60

1
2
3
4
5
6
7
8
9
10
11
12
13
14
15
16
17
18
19
20
21
22
23
24
25
26
27
28
29
30
31
32
33
34
35
36
37
38
39
40
41
42
43
44
45
46
47
48
49
50
51
52
53
54
55
56
57
58
59
60

Tables

Table 1 Parameter ranges used for sensitivity analyses. ^a The units of the ILT A factor are $10^{-11} \text{ cm}^3 \text{ molecule}^{-1} \text{ s}^{-1}$

	Theory-constrained		Experimentally-constrained	
	Lower	Upper	Lower	Upper
$E(\text{RO}_2) / \text{kJ mol}^{-1}$	-149.8	-141.4	-159.3	-132.6
$\langle \Delta E \rangle_{\text{down}} / \text{cm}^{-1}$	100.0	250.0	141.0	210.9
d (Eq2)	0	1	-0.6	0.8
ILT A ^a (Eq 3)	0.8	2	0.9	1.2
ILT n (Eq 3)	-1.0	-0.2	-1.2	-0.7
$E(\text{QOOH}) / \text{kJ mol}^{-1}$	-108.8	-100.4	-115.5	-81.5
$E(\text{TS1}) / \text{kJ mol}^{-1}$	-62.7	-35.1	-64.3	-54.9
$E(\text{TS2}) / \text{kJ mol}^{-1}$	-29.26	8.3	-38.7	-10.7

Table 2 Correlation matrix from Levenberg-Marquardt fits of the master equation input parameters to the experimental data

	$E(\text{RO}_2)$	$\langle \Delta E \rangle_{\text{down}}$	$\langle \Delta E \rangle_{\text{down exponent}}$	ILT A	ILT n	$E(\text{QOOH})$	$E(\text{TS1})$	$E(\text{TS2})$
$E(\text{RO}_2)$	1	-0.07	0.76	0.54	0.48	0.89	0.17	0.98
$\langle \Delta E \rangle_{\text{down}}$	-0.07	1	-0.13	-0.42	-0.28	0.29	-0.54	-0.04
$\langle \Delta E \rangle_{\text{down exponent}}$	0.76	-0.13	1	0.23	0.16	0.52	-0.15	0.86
ILT A	0.54	-0.42	0.23	1	0.59	0.45	0.64	0.43
ILT n	0.48	-0.28	0.16	0.59	1	0.41	0.62	0.38
$E(\text{QOOH})$	0.89	0.29	0.52	0.45	0.41	1	0.14	0.83
$E(\text{TS1})$	0.17	-0.54	-0.15	0.64	0.62	0.14	1	-0.01
$E(\text{TS2})$	0.98	-0.04	0.86	0.43	0.38	0.83	-0.01	1

Table 3: Uncertainty parameters f from both correlated (C bold) and uncorrelated (U) distributions. For the uncorrelated distributions the off diagonal elements of the Covariance matrix were assigned as zero.

	500 K 6.9×10 ¹ kPa		500 K 6.9×10 ³ kPa		700 K 9.6×10 ¹ kPa		700 K 9.7×10 ³ kPa		900 K 1.2×10 ² kPa		900 K 1.2×10 ⁴ kPa	
	C	U	C	U	C	U	C	U	C	U	C	U
R1	0.11	0.10	0.13	0.11	0.10	0.16	0.17	0.15	0.12	0.24	0.19	0.17
R2	0.34	0.41	0.28	0.37	0.36	0.41	0.28	0.39	0.35	0.39	0.28	0.39
R3	0.19	0.39	0.47	0.61	0.15	0.30	0.37	0.52	0.11	0.23	0.34	0.46
R4	0.71	0.67	0.72	0.69	0.55	0.49	0.59	0.54	0.47	0.38	0.51	0.44
R5	0.64	0.71	0.65	0.71	0.54	0.55	0.52	0.55	0.50	0.48	0.45	0.46
R6	0.44	0.81	0.66	0.74	0.24	0.58	0.31	0.66	0.18	0.46	0.23	0.53
R7	0.92	0.72	0.89	0.80	0.76	0.59	0.71	0.62	0.65	0.47	0.60	0.52
R8	0.73	0.73	0.73	0.73	0.60	0.57	0.58	0.59	0.53	0.44	0.50	0.49
R9	0.45	0.81	0.50	0.92	0.31	0.56	0.37	0.66	0.30	0.43	0.28	0.51

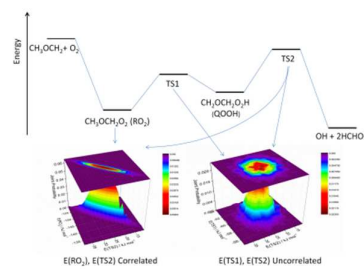
List of figure legends

Figure 1: Stationary points on the $\text{CH}_3\text{OCH}_2 + \text{O}_2$ potential energy surface from calculations at the CBS-QB3//MPW1K/aug-cc-pVTZ level of theory⁶. RO_2 is $\text{CH}_3\text{OCH}_2\text{O}_2$ and QOOH is $\text{CH}_2\text{OCH}_2\text{OOH}$.

Figure 2: Sensitivity indices for the parameters involved in the master equation modelling with theory-constrained parameter ranges (top) and experimentally-constrained parameter ranges (bottom). The labels on the top axis give the pressure at which the calculations were run in kPa and identify the type of observable: Y indicates the OH yield, L indicates the rate coefficient for CH_2OCH_3 loss, λ_1 , indicates the time constant corresponding to the longer time formation of OH and R indicates a particular elementary rate coefficient. Where the sensitivities sum to significantly less than one this can be attributed to contributions from the second order sensitivities not included. Where there is a colon between two parameters, this indicates a second order sensitivity for this pair of inputs.

Figure 3: Joint probability distributions for $E(\text{TS}_2)$ and $E(\text{RO}_2)$ for which the correlation matrix element is 0.98.

Figure 4: Joint probability distributions for $E(\text{TS}_1)$ and $E(\text{TS}_2)$ for which the correlation matrix element is -0.01.



TOC Graphic

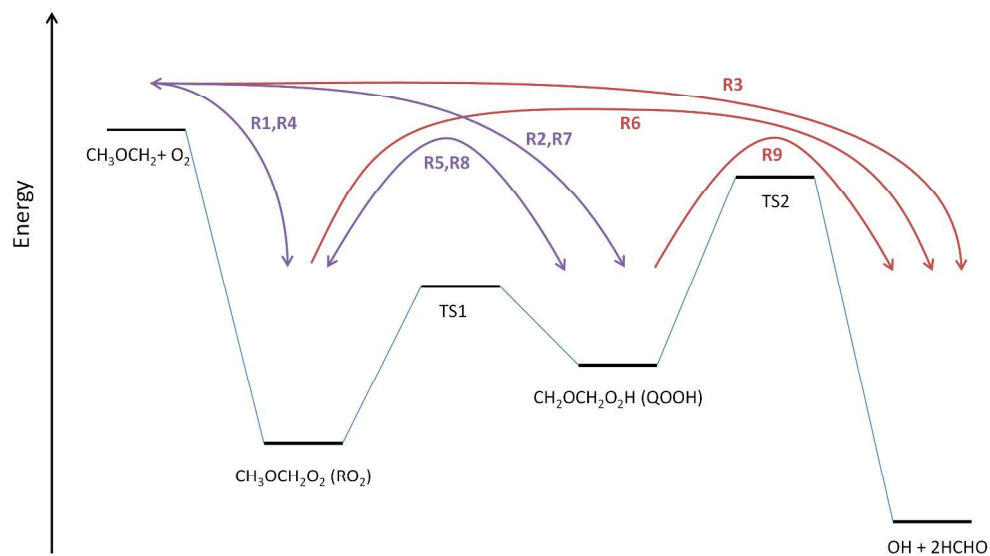


Figure 1
254x144mm (300 x 300 DPI)

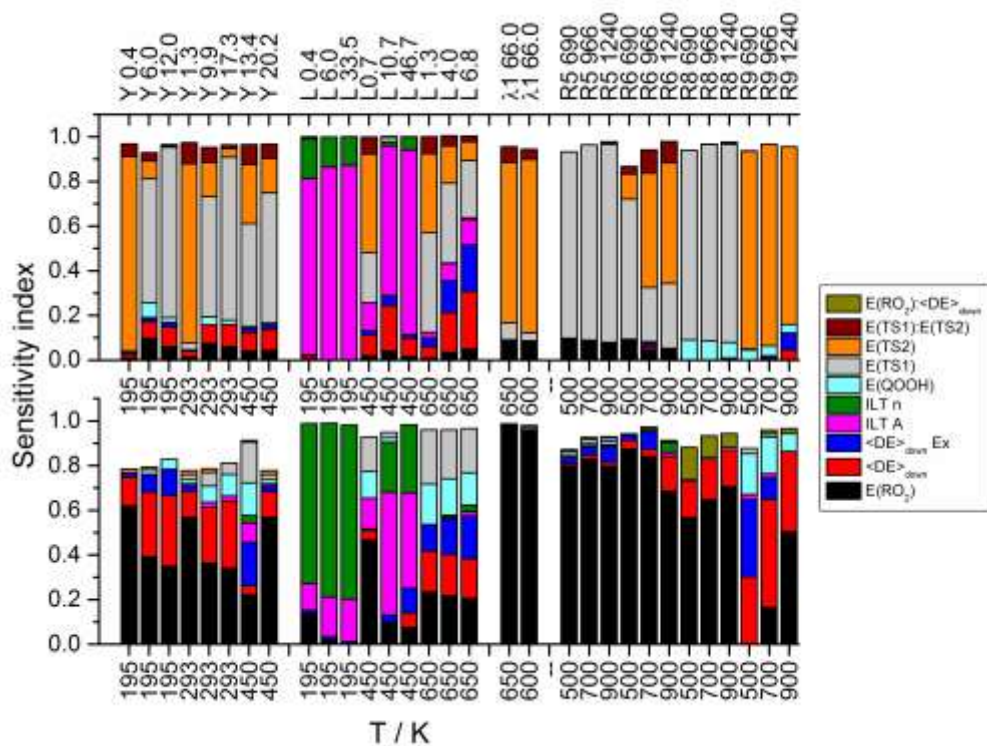


Figure 2
271x207mm (300 x 300 DPI)

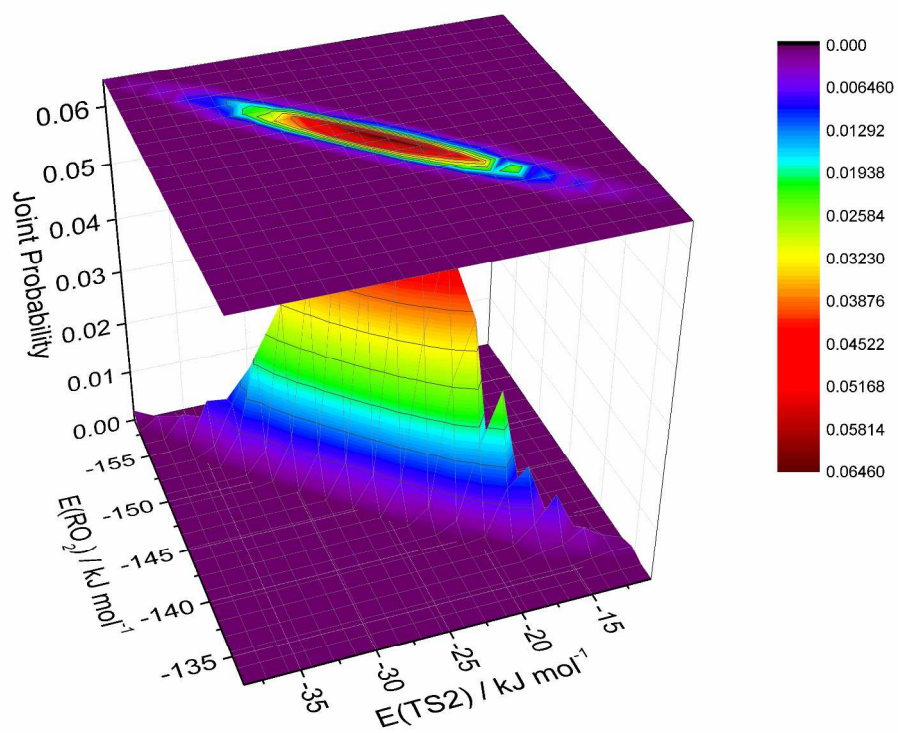


Figure 3: Joint probability distributions for $E(\text{TS2})$ and $E(\text{RO2})$ for which the correlation matrix element is 0.98.
271x207mm (300 x 300 DPI)

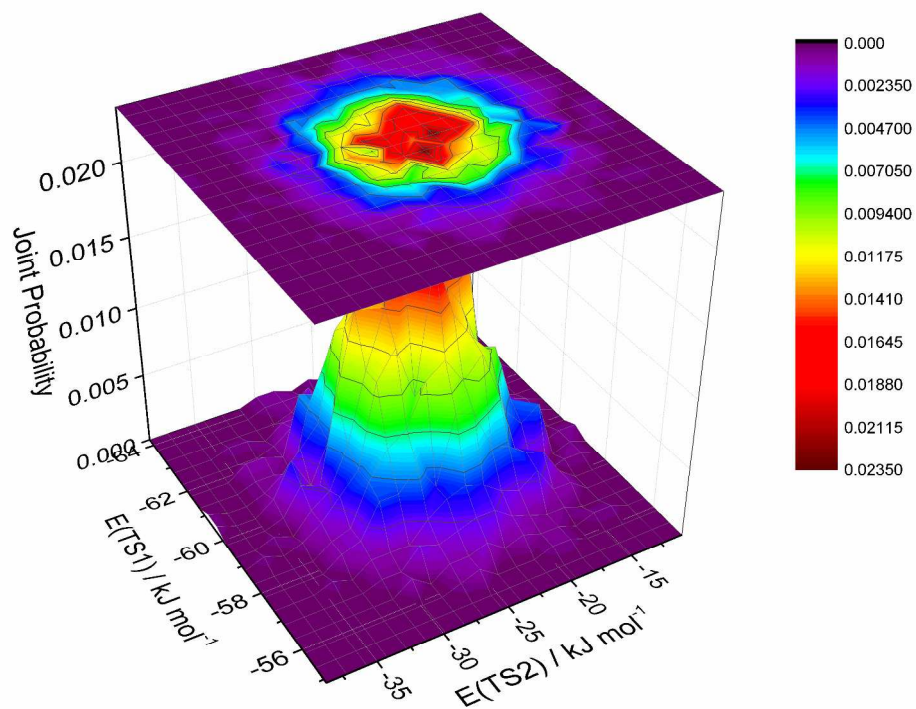


Figure 4: Joint probability distributions for $E(\text{TS1})$ and $E(\text{TS2})$ for which the correlation matrix element is -0.01.
271x207mm (300 x 300 DPI)